J. Fluid Mech. (1975), *vol.* 70, *part* 1, *pp.* 59–79
Printed in Great Britain

A theoretical and experimental study of the velocity distribution and transition to turbulence in free oscillatory flow

By CLAIRE CLARION AND ROBERT PELISSIER
Institut de Mécanique des Fluides de l'Université d'Aix Marseille

(Received 20 December 1973 and in revised form 16 December 1974)

The free oscillatory flow of a viscous fluid in a U-shaped tube is considered. A theoretical analysis (in which an axial flow is assumed and the start-up of the column is taken into account) shows, depending on the value of the similarity parameter γ, various regimes of the flow. Measurements of the velocity distribution are made using hot-film velocity probes, operated with a constant-temperature anemometer, and visualizations of the flow are performed. Experimental results are in good agreement with theoretical ones when the flow is laminar, and show the possible existence of turbulent flows. Critical values, at which the flow is disturbed over a more or less extended range of the successive oscillations, are determined for the similarity parameters γ and h_0/R.

1. Introduction

Free oscillatory viscous flow (a good illustration of which is the motion in a U-shaped tube of a liquid column, after an impulsive start from rest at an initial displacement) corresponds to a particular class of unsteady viscous flows. Analysis of the latter is very complex, since the setting in motion of the fluid column and the damping of oscillations, with other factors, must be taken into account. This problem was studied by, among other authors, J. Valensi and C. Clarion at the Institut de Mécanique des Fluides de Marseille, after Valensi (1947*a–c*) had established that the similarity parameter $\gamma = R^2\omega_p/\nu$. (ν is the coefficient of kinematic viscosity, $\omega_p = (2g/l)^{\frac{1}{2}}$ the undamped angular frequency of the motion, l and R the length and the radius of the fluid column, respectively.) This theoretical and experimental investigation showed that the flow could be either completely developed laminar flow (whatever the amplitude of oscillation), or a laminar boundary-layer flow for infinitely small amplitude, that would become, with sufficiently high values of the similarity parameter and amplitude of oscillation, first turbulent boundary-layer motion, then completely developed turbulent motion. The present work is an outgrowth of this analysis.

2. Theoretical analysis

Let us examine the laminar motion in a U-shaped tube (whose rectilinear vertical sides have a circular cross-section with a radius R) of a fluid column with a length l, displaced by a height h_0 from its position of equilibrium, then

abruptly started from rest. In order to simplify the matter, we shall not take into account the secondary phenomena occurring in the bends; and we shall limit our analysis to one side (e.g. the left), whose length is assumed to be infinite. We shall also assume that the first half-oscillation is always upward.

2.1. *Basic equations*

Let us use cylindrical co-ordinates r, θ, z (with z along the axis of the tube, positive upward), and let the origin of the co-ordinates be in the equilibrium plane of the fluid column. We shall assume that the flow is axially symmetric. The non-dimensional Navier–Stokes equations and the non-dimensional equation of continuity contain two similarity parameters γ and h_0/R. These nonlinear equations are difficult to solve. In particular, the boundary conditions on the free surface cannot be written down, since the actual shape of this surface is not known.

It is possible, however, to make a number of reasonable approximations that will simplify the analysis. A justification for these hypotheses is given by the following result of experimental investigation. We noted that, for a given experiment, the instantaneous axial velocity profiles are similar along the fluid column away from the small region affected by the ends, and that, on the other hand, the free surface keeps an unchanging and roughly plane shape as time progresses. We are thus led to the following scheme. (i) Near the free surface (by assumption plane), there is a thin fluid layer, similar to a boundary layer in which the radial velocity component cannot be neglected. (ii) Away from this region, the flow is axial. Under these assumptions, the non-dimensional governing equations have the form

$$\frac{\partial p'^{X}}{\partial r'} = 0, \quad \frac{\partial W'}{\partial t'} - \frac{1}{\gamma}\left(\frac{\partial^2 W'}{\partial r'^2} + \frac{1}{r'}\frac{\partial W'}{\partial r'}\right) = -\frac{\partial p'^{*}}{\partial z'}, \quad \frac{\partial W'}{\partial z'} = 0, \qquad (1)\text{–}(3)$$

where $$W' = \frac{W}{\omega_p h_0}, \quad p'^{*} = \frac{h_0}{R}\frac{p+\rho g z}{\rho(\omega_p h_0)^2}, \quad r' = \frac{r}{R}, \quad z' = \frac{z}{R}, \quad t' = \omega_p t.$$

Here t denotes time, W the component of the fluid velocity in the axial direction, p the pressure, ρ the density and g the acceleration due to gravity.

We have to supplement (1)–(3) with proper boundary and initial conditions. These are

$$\left.\begin{aligned} &t' \leqslant 0, \quad 0 \leqslant r' \leqslant 1, \quad \text{(i)}\ W' = 0, \quad \text{(ii)}\ h' = -h_0, \\ &t' > 0, \quad r' = \pm 1, \quad \text{(iii)}\ W' = 0, \quad \text{(iv)}\ \text{free surface replaced by plane } z = h, \end{aligned}\right\} \qquad (4)$$

where $$h = (2/R^2)\int_0^R r\,dr \int_{t_0}^{t} W\,dt; \qquad (5)$$

after the release of the fluid column $h = 0$ at $t = t_0$.

Let the pressure gradient be represented by the series

$$-\frac{\partial p'^{*}}{\partial z'} = \sum_{n=1}^{\infty} B_n \exp(it'\omega_n/\omega_p). \qquad (6)$$

B_n and ω_n/ω_p are complex functions of the sole parameter γ. The general solution of (1)–(3), satisfying the boundary condition (iii), is the well-known relation between unsteady velocity profile and pressure gradient determined by Sexl

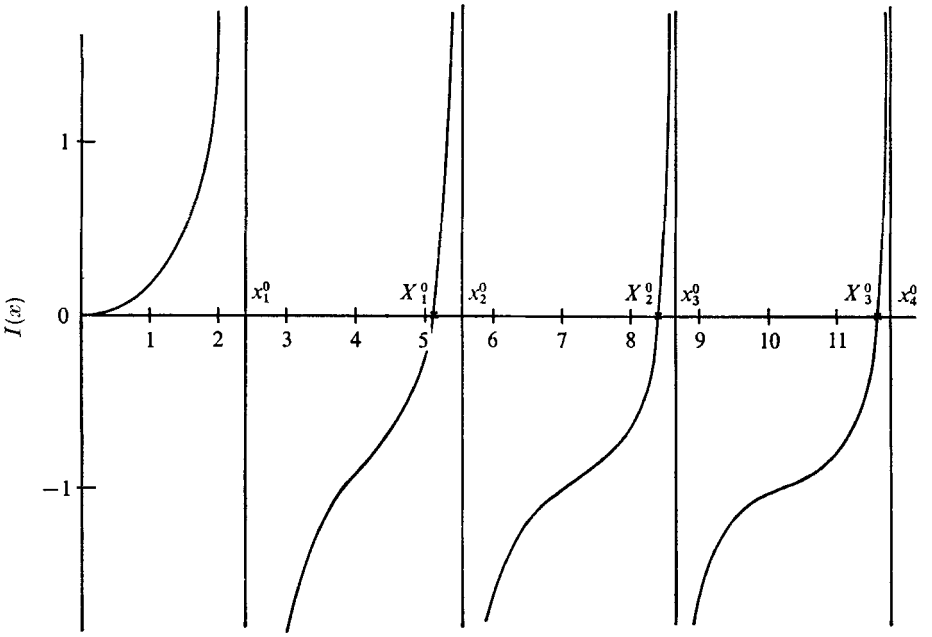

FIGURE 1. Graph of function $I(x)$. x_m^0 roots of $J_0(x) = 0$.

(1930), then by Womersley (1955) and Uchida (1956) in the case of pulsating flow. Consequently we have

$$\frac{W}{\omega_p h_0} = \sum_{n=1}^{\infty} -i \frac{B_n}{\omega_n/\omega_p} \left[1 - \frac{J_0([-i\gamma\omega_n/\omega_p]^{\frac{1}{2}} r/R)}{J_0([-i\gamma\omega_n/\omega_p]^{\frac{1}{2}})}\right] \exp(it'\omega_n/\omega_p). \tag{7}$$

J_0 is the Bessel function of first kind and zero order. By integrating the pressure gradient all round the U-tube, and taking (5) into consideration, it is easy to obtain

$$\frac{\partial p'^*}{\partial z'} = \frac{h}{h_0} = \sum_{n=1}^{\infty} -\frac{B_n}{(\omega_n/\omega_p)^2} \left[1 - 2\frac{J_1([-i\gamma\omega_n/\omega_p]^{\frac{1}{2}})}{[-i\gamma\omega_n/\omega_p]^{\frac{1}{2}} J_0[-i\gamma\omega_n/\omega_p]^{\frac{1}{2}})}\right] \exp(it'\omega_n/\omega_p). \tag{8}$$

Identifying (6) and (8), we find that ω_n/ω_p is a solution of

$$(\omega_n/\omega_p)^2 = 1 - \frac{2J_1([-i\gamma\omega_n/\omega_p])}{[-i\gamma\omega_n/\omega_p]^{\frac{1}{2}} J_0([-i\gamma\omega_n/\omega_p]^{\frac{1}{2}})}. \tag{9}$$

J_1 is the Bessel function of first kind and first order.

2.2. *Discussion of* (9)

We notice that the roots of (9) can be only imaginary or complex. Let us first examine the imaginary roots. Set

$$\frac{\omega_n}{\omega_p} = i\frac{\lambda_n}{\omega_p}, \quad x = [\gamma\lambda_n/\omega_p]^{\frac{1}{2}} \quad (x \geqslant 0), \quad I(x) = \frac{2}{x}\frac{J_1(x)}{J_0(x)} - 1.$$

λ_n/ω_p is the damping factor of the corresponding partial. Then (9) is reduced to

$$(\lambda_n/\omega_p)^2 = I(x), \quad x = [\gamma\lambda_n/\omega_p]^{\frac{1}{2}}. \tag{10}$$

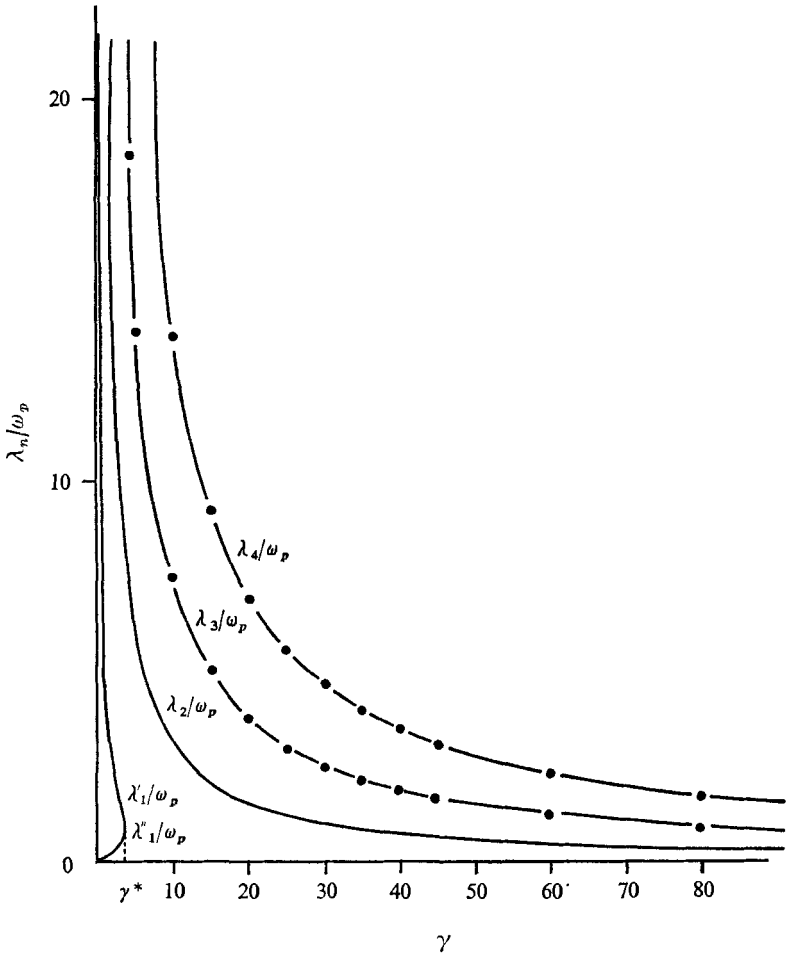

FIGURE 2. λ_n/ω_p as a function of γ. ——, computed values; ●, values given by approximate expression (11).

It is clear, from the graph of the function $I(x)$ in figure 1, that, to each positive value of $I(x)$, correspond an infinity of values of x (denoted by $x_1, x_2, \ldots, x_m$), then an infinity of couples $(\lambda_n/\omega_p, \gamma)$, given by (10). $x_1 \in [0, x_1^0[$ and

$$x_m \in [X_m, x_{m+1}[,$$

where X_m are the roots of $I(x) = 0$, and x_m^0 the roots of $J_0(x) = 0$.

Let us examine the functions $\gamma(\lambda_n/\omega_p, x)$. The derivative $d\gamma/d(\lambda_n/\omega_p)$ is equal to zero for $x = x^*$ $(0 \leqslant x^* < x_1^0)$. It is positive for $0 \leqslant x < x^*$, negative for $x > x^*$. Then, for $x \geqslant x_1^0$ (i.e. $n \geqslant 2$), γ decreases with increasing λ_n/ω_p; but, for $x < x_1^0$ (i.e. for $n = 1$), γ first increases, then decreases with increasing λ_1/ω_p.

The graphs of λ_n/ω_p as a function of γ are given in figure 2, for $n = 1, 2, 3, 4$. ($\gamma^* \simeq 3{\cdot}436$ is the corresponding value of $x = x^*$.) For $0 < \gamma \leqslant \gamma^*$, to $n = 1$ correspond two roots λ'_1/ω_p and λ''_1/ω_p; and, to each value of $n \geqslant 2$, corresponds a root λ_n/ω_p. For $\gamma > \gamma^*$, for $n = 1$ we have no root; but to each $n \geqslant 2$ corres-

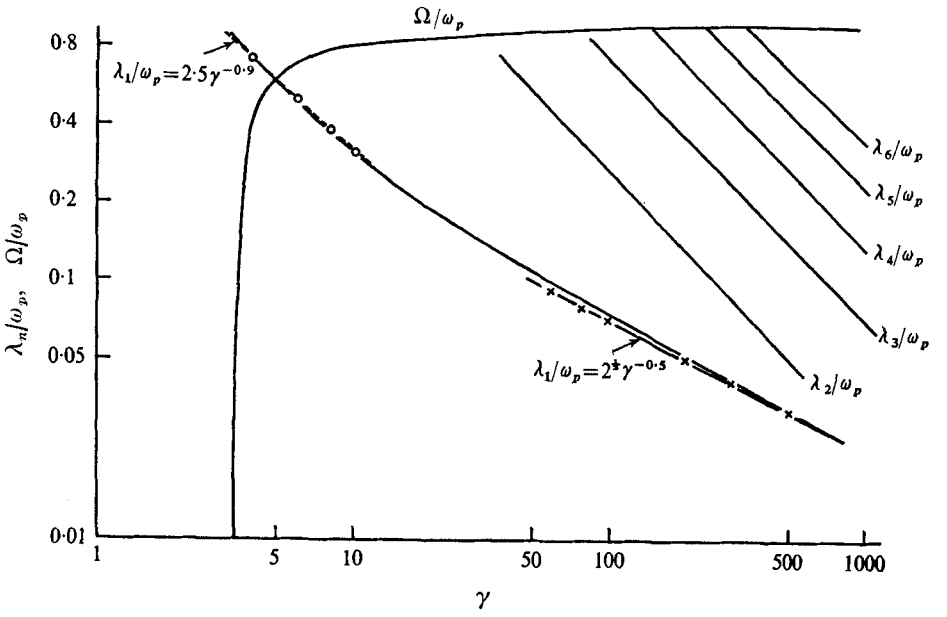

FIGURE 3. Logarithmic representation of Ω/ω_p and λ_n/ω_p as a function of γ.

ponds a root λ_n/ω_p, as for $0 < \gamma \leqslant \gamma^*$. From the asymptotic expansions of Bessel functions, we may obtain the approximate expression for $n > 2$

$$\lambda_n/\omega_p = (n\pi - \tfrac{1}{4}\pi)^2/\gamma. \tag{11}$$

In figure 2, the values of λ_n/ω_p given by (11) are quite in agreement with those given by the computation of the roots. Let us now examine the complex roots of (9).

Setting $\omega_n/\omega_p = \Omega_n/\omega_p + i\lambda_n/\omega_p$ and $[-i\gamma\omega_n/\omega_p]^{\frac{1}{2}} = \rho\exp(i\theta)$, (9) is reduced to

$$\frac{\rho^4}{\gamma^2}\exp i(4\theta+\pi) = 1 - \frac{2J_1(\rho\exp(i\theta))}{\rho\exp(i\theta)\,J_0(\rho\exp(i\theta))}.$$

If, for a given value of ρ, θ is a root of this equation, $\pi+\theta$, $\pi-\theta$ and $-\theta$ are also roots. To these four values of θ correspond two roots of (9)

$$\pm\,\Omega/\omega_p + i\lambda_1/\omega_p.$$

$T = 2\pi/\Omega$ is the pseudo period of the flow. It is easy to show that these roots exist only for $\gamma > \gamma^*$, and that they are unique. Then, for $\gamma \leqslant \gamma^*$, the flow is aperiodic; for $\gamma > \gamma^*$, it is oscillatory. The logarithmic representation of Ω/ω_p and λ_n/ω_p as a function of γ is plotted in figure 3. There is good agreement between the values of λ_1/ω_p and the corresponding ones given by the empirical expressions determined from experiments (Clarion 1955)

$$\lambda_1/\omega_p = 2{\cdot}5\gamma^{-0{\cdot}9}, \quad 3{\cdot}46 < \gamma < 25; \quad \lambda_1/\omega_p = 2^{-\frac{1}{2}}\gamma^{-0{\cdot}5}, \quad \gamma > 46.$$

2.3. *Velocity and damping factor*

It follows from the discussion of (9), and from (7), that the general solution of (1)–(3), satisfying the initial and boundary conditions (4), is

$$\frac{W}{\omega_p h_0} = -k\Bigg\{\sum_{m=1}^{\infty}(a_{0_m}+\Lambda a_{1_m})\exp\,(-\Omega t\lambda_1\omega_p/(\omega_p\Omega))\frac{J_0(x_m^0(r/R)}{x_m^0 J_1(x_m^0)} + \sum_{n=2}^{\infty}\Lambda D_n\exp(-\Omega t\lambda_n\omega_p/(\omega_p\Omega))\sum_{m=1}^{\infty}\frac{\gamma\lambda_n/\omega_p}{\gamma\lambda_n/\omega_p-(x_m^0)^2}\frac{J_0(x_m^0(r/R))}{x_m^0 J_1(x_m^0)}\Bigg\}. \quad (12)$$

Λ, k, D_n are coefficients, functions of the sole parameter γ, determined by the initial conditions

$$a_{0_m} = \frac{[(\lambda_1/\omega_p)^2+(\Omega/\omega_p)^2-x_m^{02}\gamma^{-1}\lambda_1/\omega_p]\cos\Omega t-\gamma^{-1}(x_m^0)^2\sin\Omega t\Omega/\omega_p}{[\lambda_1/\omega_p-(x_m^0)^2\gamma^{-1}]^2+(\Omega/\omega_p)^2},$$

$$a_{1_m} = \frac{[(\lambda_1/\omega_p)^2+(\Omega/\omega_p)^2-(x_m^0)^2\gamma^{-1}\lambda_1/\omega_p]\sin\Omega t+\gamma^{-1}(x_m^0)^2\cos\Omega t\Omega/\omega_p}{[\lambda_1/\omega_p-(x_m^0)^2\gamma^{-1}]^2+(\Omega/\omega_p)^2},$$

valid for $\gamma > \gamma^*$ (i.e. when the flow is oscillatory); and

$$\frac{W}{\omega_p h_0} = -k\Bigg\{\exp(-\omega_p t\lambda_1'/\omega_p)\sum_{m=1}^{\infty}\frac{\gamma\lambda_1'/\omega_p}{\gamma\lambda_1'/\omega_p-(x_m^0)^2}\frac{J_0(x_m^0(r/R)}{x_m^0 J_1(x_m^0)} + \Lambda\exp(-\omega_p t\lambda_1''/\omega_p)\sum_{m=1}^{\infty}\frac{\gamma\lambda_1''/\omega_p}{\gamma\lambda_1''/\omega_p-(x_m^0)^2}\frac{J_0(x_m^0(r/R)}{x_m^0 J_1(x_m^0)} + \sum_{m=2}^{\infty}\Lambda D_n\exp(-\omega_p t\lambda_n/\omega_p)\sum_{m=1}^{\infty}\frac{\gamma\lambda_n/\omega_p}{\gamma\lambda_n/\omega_p-(x_m^0)^2}\frac{J_0(x_m^0(r/R))}{x_m^0 J_1(x_m^0)}\Bigg\}, \quad (13)$$

valid for $\gamma \leqslant \gamma^*$ (i.e. when the flow is aperiodic). As regards oscillatory flows, the damping value between the pth and the $(p+1)$th oscillation is given by the relation $h_{(2p-1)\pi}/h_{(2p+1)\pi}$, where

$$\frac{h}{h_0} = -k\Bigg\{\sum_{m=1}^{\infty}\frac{\exp(-\Omega t\lambda_1\omega_p/(\omega_p\Omega))\,[(a_{1_m}-\Lambda a_{0m})\,\Omega/\omega_p-(a_{0_m}+\Lambda a_{1_m})\lambda_1/\omega_p]}{(x_m^0)^2\,[(\lambda_1/\omega_p)^2+(\Omega/\omega_p)^2]} - \sum_{n=2}^{\infty}\Lambda D_n\exp(-\Omega t\lambda_n\omega_p/(\omega_p\Omega))\sum_{m=1}^{\infty}\frac{\gamma}{(x_m^0)^2(\gamma\lambda_n/\omega_p-(x_m^0)^2)}\Bigg\}. \quad (14)$$

When the aperiodic partial terms are not taken into account, one can easily check:

$$h_{(2p-1)\pi}/h_{(2p+1)\pi} = \exp(2\pi\lambda_1/\Omega).$$

Solutions (12)–(14) are very complex, and can be exploited only by numerical analysis.

3. Presentation and discussion of numerical results

3.1 *Velocity profile*

Calculations of $W/(\omega_p h_0)$, given by solutions (12) and (13), and of h/h_0, given by solution (14), have been made for twenty values of γ ($1 \leqslant \gamma \leqslant 400$), ten values of $\omega_p t$ ($0 \leqslant \omega_p t \leqslant 30$) in the aperiodic flow, and fifteen values of Ωt ($0 \leqslant \Omega t \leqslant 3\pi$) in the oscillatory flows. The value of $\Delta r/R$ was chosen to be 0·025. From these results we obtain, for a given value of γ, the evolution at increasing times of the

instantaneous velocity profiles. A number of examples corresponding to representative values of γ are presented in figures 4–7.

Examination of the profiles suggests that the typical profiles shapes observed should be classified into the following groups. We examine first the profiles for which the velocity is either always positive or always negative in the section, from the wall to the axis, or from the wall to the boundary of the central core, when the profiles are not fully developed. (This is the case at the start, up to a value of Ωt which is an increasing function of γ.) In group (i), the modulus of velocity increases monotonically. (See e.g. figure 5: $\gamma = 15{\cdot}3$, $\Omega t = \frac{1}{2}\pi$.) In group (ii), the modulus of velocity reaches a maximum, then decreases. (See e.g. figure 6: $\gamma = 177$, $\Omega t = \frac{3}{2}\pi$.) In group (iii), the modulus of velocity reaches a maximum, then a minimum, then increases. (See e.g. figure 6: $\gamma = 177$, $\Omega t = \frac{5}{2}\pi$.) And so on. When the modulus of velocity is reduced to zero at a point in the section defined by $r = r_I$, the corresponding profile is termed a *reverse-flow* profile. In this case, the modulus of velocity reaches a maximum with

$$r_I < r \leqslant R.$$

With $r \leqslant r_I$, the profile shape is similar to the nth previously defined shape. The profile is therefore classified into the group $n+1$. (See e.g. figure 5: $\gamma = 15{\cdot}3$, $\Omega t = \pi$.)

The evolution of the shape of the instantaneous velocity profiles according to this classification is summarized in figure 8, corresponding to $0 \leqslant \Omega t \leqslant 3\pi$ and $\gamma^* < \gamma < 140$. (In aperiodic flow profiles belong to group (i).) We note reverse flow profiles from $\Omega t = k\pi - \phi$, where $0 < \phi < \frac{1}{4}\pi$, $\phi = 0{\cdot}85\pi$ for $\gamma = 15$, $\phi \simeq \frac{1}{4}\pi$ for $\gamma > 38$ (the values of Ωt corresponding to $k = 1, 2, 3$ are, respectively, Ωt_2, Ωt_4, Ωt_6), up to $\Omega t = k\pi + \epsilon$, where $0 < \epsilon < \frac{1}{6}\pi$, $\epsilon \simeq \frac{1}{6}\pi$ for $\gamma \simeq 46$. At Ωt_2, Ωt_4, Ωt_6, the sign of the velocity gradient at the wall changes, $(\partial w'/\partial r')_{r'=1} = 0$, an extremum of the velocity appears near the wall, and the group of the profile changes from n to $n+1$. Moreover, the modulus of the velocity of a fully developed profile reaches an extremum on the axis of the tube. This extremum becomes a minimum if it was a maximum, and vice versa; and the group of the profile changes from $n+1$ to n at Ωt_3 ($\pi < \Omega t_3 \leqslant 2\pi$) and Ωt_5 ($2\pi < \Omega t_5 \leqslant 3\pi$), corresponding to the condition $(\partial^2 w'/\partial r'^2)_{r'=0} = 0$ (Ωt_3 and Ωt_5 are, respectively, defined for $8 \leqslant \gamma \leqslant 46$ and $8 \leqslant \gamma \leqslant 140$). From figure 8, when the first up motion occurs, the profile belongs to group (i) up to Ωt_2 whatever γ; and, during the first down motion, the profile may belong to group (i) only if $\gamma < 38$, and in that case between Ωt_3 and Ωt_4 only.

It seems interesting to compare these results with those relative to a flow oscillating under a sinusoidal pressure gradient $-(1/\rho)\,\partial p/\partial z = C\exp(i\Omega t)$. ($C$ and Ω are real, the flow being considered a long time after the start-up.) The velocity can be expressed in the form, given by Sexl,

$$W = -\frac{iC}{\Omega}\left[1 - \frac{\operatorname{ber} q_1 + i \operatorname{bei} q_1}{\operatorname{ber} q + i \operatorname{bei} q}\right]\exp(i\Omega t),$$

where

$$\gamma = R^2\Omega/\nu, \quad [\gamma r^2/R^2]^{\frac{1}{2}} = q_1, \quad \gamma^{\frac{1}{2}} = q,$$
$$J_0[-iq_1]^{\frac{1}{2}} = \operatorname{ber} q_1 + i \operatorname{bei} q_1.$$

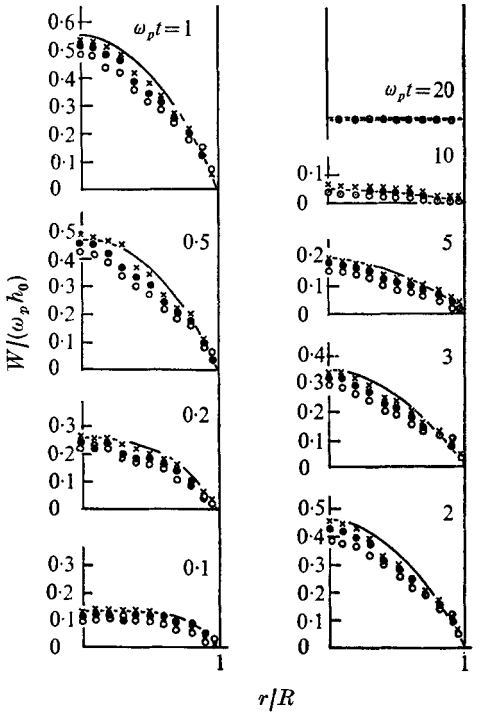

FIGURE 4. Axial instantaneous velocity profiles, $\gamma = 2{\cdot}04$ (aperiodic flow). ——, theory. Experiment, h_0/R: ×, 4; ●, 10; ○, 40.

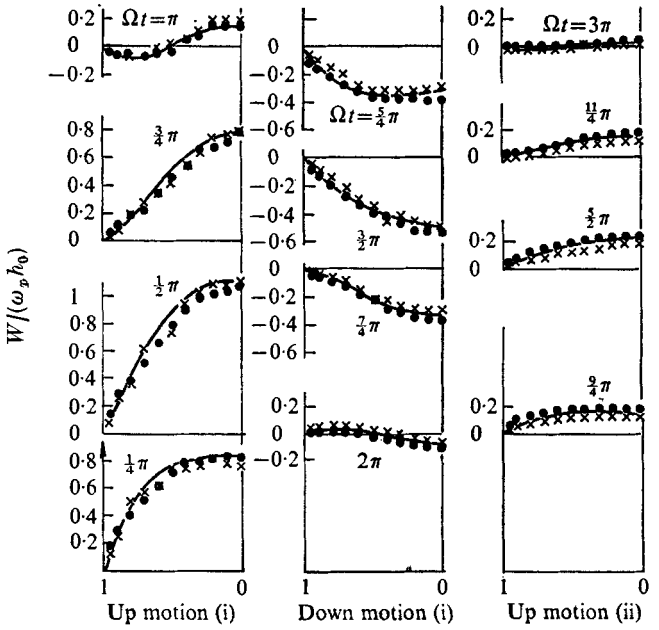

FIGURE 5. Axial instantaneous velocity profiles, $\gamma = 15{\cdot}3$ (first regime). ——, theory. Experiment, h_0/R: ●, 4; ×, 50.

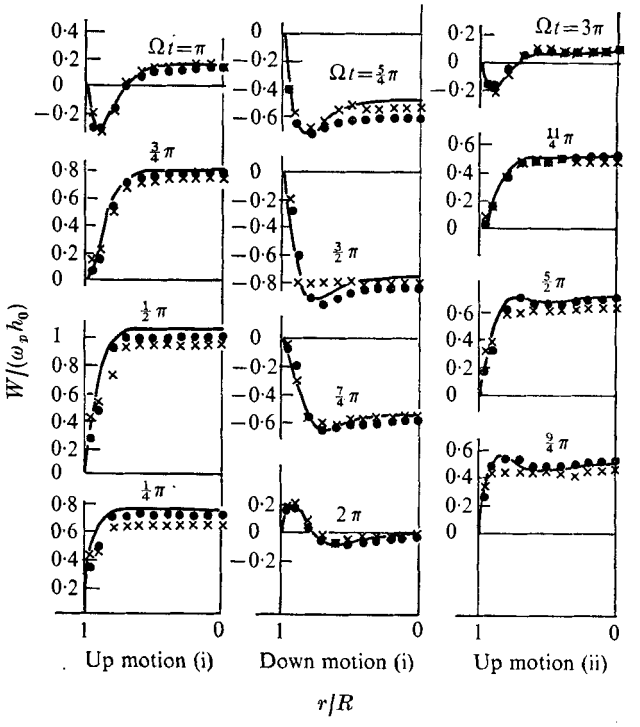

FIGURE 6. Axial instantaneous velocity profiles, $\gamma = 177$ (second regime). ——, theory. Experiment, h_0/R: ●, 4; ×, 25.

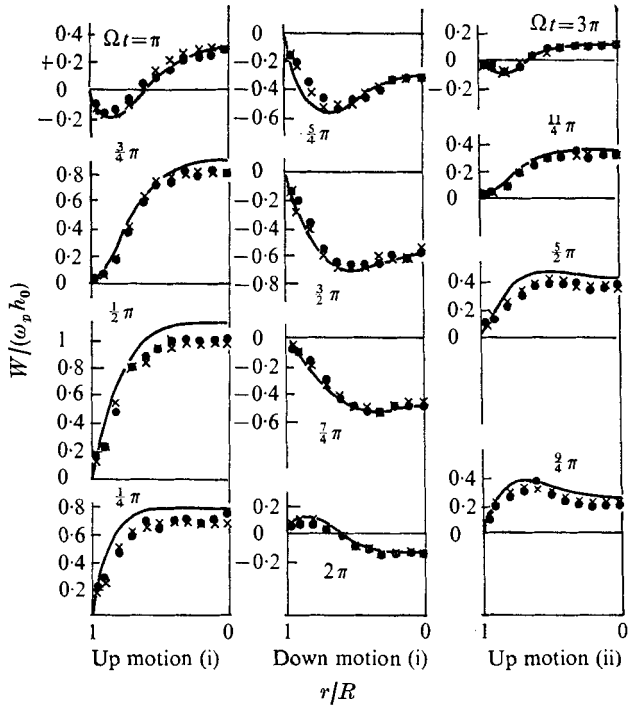

FIGURE 7. Axial instantaneous velocity profiles, $\gamma = 42$ (intermediate regime). ——, theory. Experiment, h_0/R: ●, 4; ×, 25.

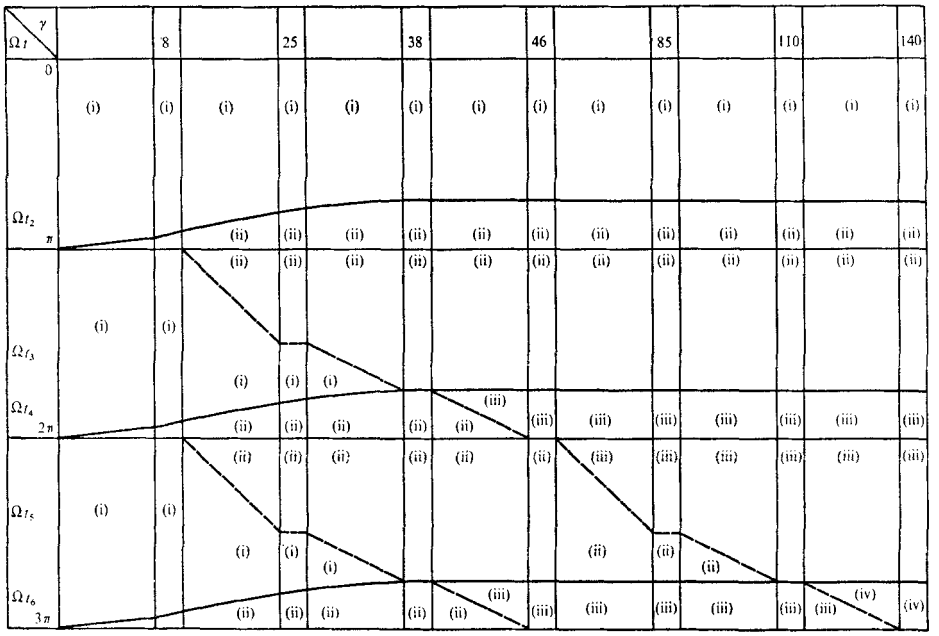

FIGURE 8. Evolution of shape of instantaneous velocity profiles, according to classification into groups, for $0 \leqslant \Omega t \leqslant 3\pi$ and $\gamma^* < \gamma < 140$. (In aperiodic flow, profiles belong to group (i).) – – –, Ωt_3, Ωt_5; ——, Ωt_2, Ωt_4, Ωt_6.

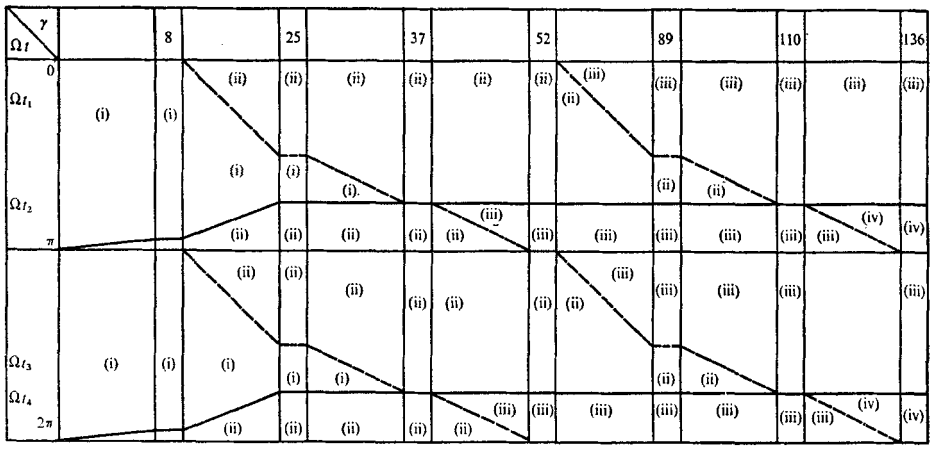

FIGURE 9. Evolution of shape of instantaneous velocity profiles, according to classification into groups, for Sexl's expression of velocity, one oscillation $0 \leqslant \Omega t \leqslant 2\pi$, and $0 < \gamma < 136$. – – –, Ωt_1, Ωt_3; ——, Ωt_2, Ωt_4.

The evolution of the shape of the instantaneous velocity profiles of this motion, according to the classification adopted earlier, is summarized in figure 9, during one oscillation $0 \leqslant \Omega t \leqslant 2\pi$, and for $0 < \gamma < 136$.

For a given value of γ, the group of the profile changes from n to $n+1$ at Ωt_2 and Ωt_4, corresponding to $(\partial w'/\partial r')_{r'=1} = 0$, and from $n+1$ to n at Ωt_1 and Ωt_3, corresponding to $(\partial^2 w'/\partial r'^2)_{r'=0} = 0$. It is easy to show that $\Omega t_1 = \frac{1}{2}\pi$ and $\Omega t_3 = \frac{3}{2}\pi$ for $\mathrm{bei}\, q = 0$, corresponding to $\gamma = 25$, 89, 193, that $\Omega t_1 = \pi$ and

$\Omega t_3 = 2\pi$ for $\mathrm{ber}\, q = 0$, corresponding to $\gamma = 8, 52, 136$, and that $\Omega t_1 \simeq \Omega t_2$ and $\Omega t_3 \simeq \Omega t_4$ for $\mathrm{ber}\, q = \mathrm{bei}\, q$, corresponding to $\gamma = 37, 110$. The characteristic values of γ given in figure 8 are quite in agreement with the corresponding values for the oscillating flow given in figure 9. Moreover, the influence of the start-up in this classification is noticeable up to a value of Ωt which increases with γ. Let us now study this initial flow.

3.2. *Boundary layer*

It is well known (Batchelor 1967) that, at start-up, the flow is entirely irrotational. Then vorticity is produced at the wall, and diffused away. A boundary layer is formed. Adopting a definition of boundary-layer thickness δ (e.g. that distance from the wall beyond which the modulus of velocity remains within 1 % of the value on the axis), we can distinguish boundary-layer and fully developed profiles.

Since the sign of the velocity gradient at the wall changes in the vicinity of $\Omega t \simeq k\pi - \phi$, the vorticity at the wall is alternately positive and negative. It is easy to show that γ is related to the ratio of the tube radius to the distance vorticity diffuses in one pseudo period. Consequently, at the start profiles are blunt up to Ωt_l, with Ωt_l increasing as γ increases. At later times $\Omega t > \Omega t_l$, profiles are fully developed, but, at a given Ωt, they are very different, depending on the value of γ. In particular, for small γ (see e.g. figure 5, $\gamma = 15{\cdot}3$), the velocity varies continuously from the axis to the wall; and, for large γ (see e.g. figure 6, $\gamma = 177$), the velocity varies slowly in some central region, then falls rapidly to zero. Since

$$(\partial^2 w'/\partial r'^2)_{r'=0} = 0 \quad \text{for} \quad \Omega t \leqslant \Omega t_l, \quad (\partial^2 w'/\partial r'^2)_{r'=0} \neq 0 \quad \text{for} \quad \Omega t > \Omega t_l,$$

it follows that

$$\Omega t_l = \Omega t_1 \quad \text{for} \quad 0 < \Omega t_l \leqslant \pi, \quad \Omega t_l = \Omega t_2 \quad \text{for} \quad \pi < \Omega t_l \leqslant 2\pi,$$

and so on. Ωt_1 and Ωt_2 are determined in figures 8 and 9. The size of the central core is, for a given value of Ωt, an increasing function of γ, and for a given value of γ, a decreasing function of Ωt.

The logarithmic representation of the boundary-layer relative thickness as a function of γ, with Ωt as parameter, is given in figure 10. For a given value of Ωt, the representative curve is formed by two straight lines of different slopes, intersecting at $\gamma = 25$. The expression for δ/R as a function of γ and Ωt is consequently different for $\gamma \leqslant 25$ or $\gamma > 25$. For $\gamma \leqslant 25$, we obtain

$$\delta/R = 5{\cdot}8\gamma^{-0{\cdot}6}(\Omega t)^{\frac{1}{2}}. \tag{15}$$

This equation can be rewritten in the form

$$\delta = k(\nu t)^{\frac{1}{2}},$$

where

$$k = 5{\cdot}8\gamma^{-0{\cdot}1}(\Omega/\omega_p)^{\frac{1}{2}}. \tag{15a}$$

It is easy to see that $k \simeq 4$:

$$k = 3{\cdot}91 \quad \text{for} \quad \gamma = 25; \quad k = 4{\cdot}17 \quad \text{for} \quad \gamma = 5.$$

Let us compare this formula with the corresponding one given by Stokes's first problem of an instantaneously accelerated flat plate:

$$\delta = 4(\nu t)^{\frac{1}{2}}. \tag{16}$$

The excellent agreement between (15a) and (16) can be explained by the fact that, for $\gamma \leqslant 25$, the boundary layer develops during the accelerated phase of the first up motion. When $\gamma > 25$, the boundary-layer thickness is proportional to the square root of the time only at the start-up ($0 \leqslant \Omega t \leqslant 0{\cdot}04$).

3.3. *Skin friction on the wall*

The mean skin-friction coefficient $\bar{C}_f$ is defined by

$$\bar{C}_f = 2\left(\gamma\frac{h_0}{R}\right)^{-1}\overline{\left[\frac{\partial W/(\omega_p h_0)}{\partial r/R}\right]}_{r/R=1}\overline{\left(\frac{W_m}{\omega_p h_0}\right)^{-2}}. \tag{17}$$

W_m is the instantaneous mean velocity in the section, and the subscript on the quantity considered designates half the sum of the mean value of the quantity between 0 and π, and of the mean value between π and 2π. Let us define the Reynolds number

$$\mathscr{R}_m = \frac{R\overline{W}_m}{\nu} = \frac{\overline{W}_m}{\omega_p h_0}\gamma\frac{h_0}{R}.$$

$\mathscr{R}_m$ is obviously a product of h_0/R and a function of γ. The curves of the logarithmic representation of $\bar{C}_f$ as a function of $\mathscr{R}_m$ with γ as a parameter, plotted in figure 11, are straight lines with a -1 slope. If $\gamma > 25$, to each value of γ corresponds a straight line, leading to

$$\bar{C}_f = (2{\cdot}4\gamma^{0{\cdot}4})\mathscr{R}_m^{-1}. \tag{18a}$$

If $8 < \gamma \leqslant 25$, whatever the value of γ, the straight line remains the same, leading to

$$\bar{C}_f = 8{\cdot}75\mathscr{R}_m^{-1}. \tag{18b}$$

($\gamma^* < \gamma \leqslant 8$ is a transition domain between aperiodic and periodic flows.)

From these results, it follows that $\mathscr{R}_m$ appears as a relevant parameter of the flow only for $\gamma \leqslant 25$. For $\gamma > 25$, two parameters, $\mathscr{R}_m$ and γ (or $\mathscr{R}_m$ and h_0/R) are necessary to determine $\bar{C}_f$. Moreover, we can draw, for $\gamma > 25$ (figure 11), the curves of the logarithmic representation of $\bar{C}_f$ as a function of $\mathscr{R}_m$ with h_0/R as a parameter. These curves are straight lines with a $-0{\cdot}7$ slope. The -1 slope straight lines and the $-0{\cdot}7$ slope straight lines form a network that makes it possible to determine the value of $\bar{C}_f$ corresponding to a chosen value of γ and of h_0/R. Finally, (18b) agrees with the laminar Poiseuille flow result $C_f = 8\mathscr{R}^{-1}$.

3.4. *Damping of oscillatory flows*

The damping given by (14) is constant during the successive oscillations when $\gamma \leqslant 25$; but it decreases at the beginning of the motion, then keeps a constant value when $\gamma > 25$.

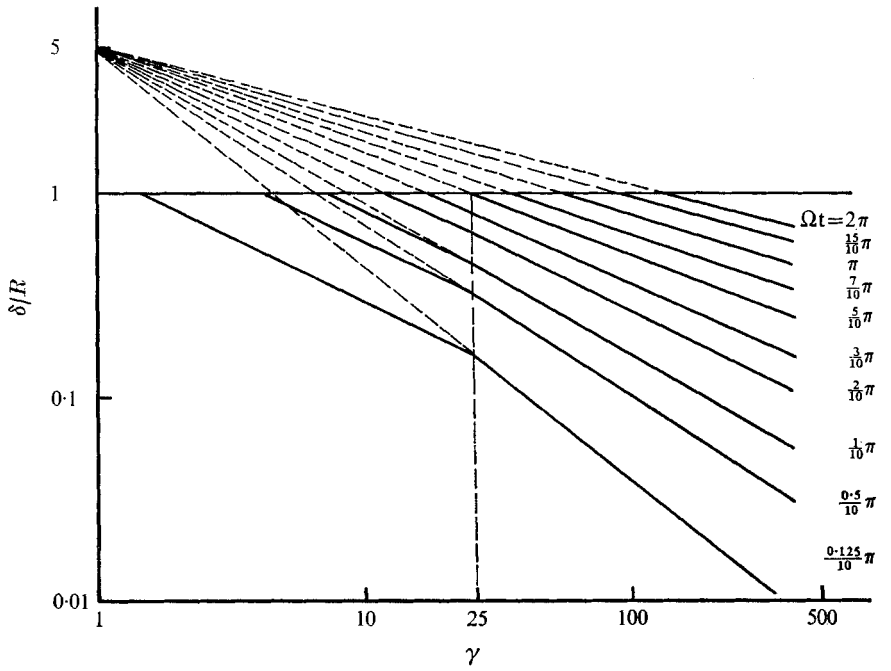

FIGURE 10. Boundary-layer relative thickness δ/R as a function of γ, for different values of Ωt.

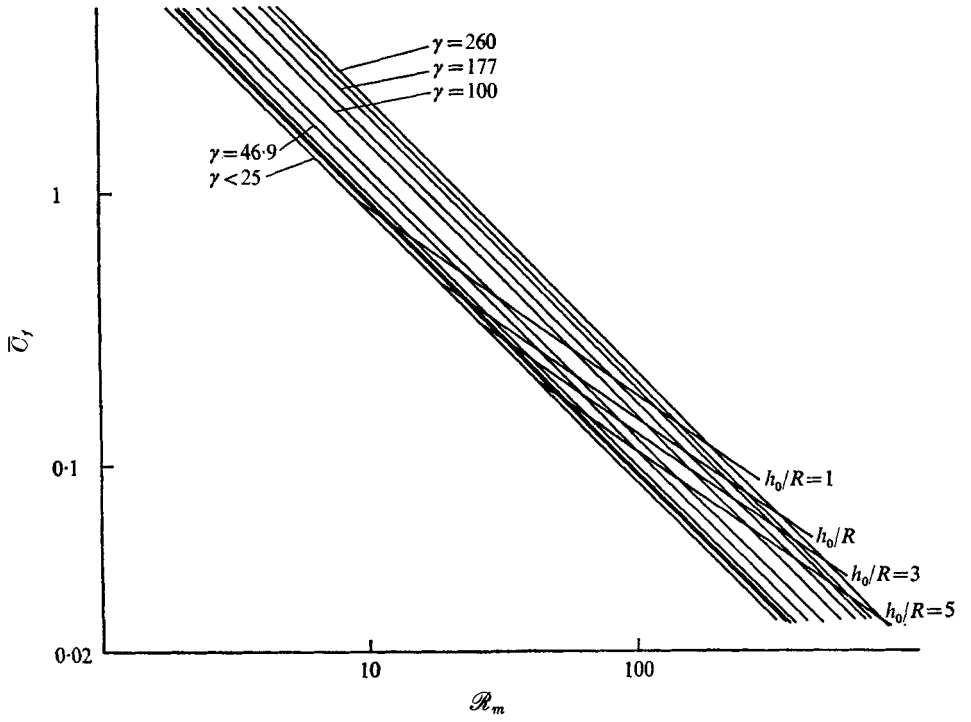

FIGURE 11. Mean skin-friction coefficient $\overline{C}_f$ as a function of $\mathscr{R}_m$, for different values of h_0/R and γ.

3.5. *Stability criterion*

A necessary condition for instability of two-dimensional steady flows was obtained by Rayleigh (1895). An improvement of the condition was subsequently given by Hoiland (1953). Batchelor & Gill (1962) established this condition for steady axisymmetric flows, and Conrad & Criminale (1965*a*, *b*) for unsteady two-dimensional flows. An attempt is made here to generalize the criterion to the present free oscillatory flow, which belongs to the class of unsteady parallel axisymmetric flows.

A three-dimensional disturbance characterized by the pressure p^X and the velocity of components $u^X(r,z,t)$, $v^X(r,z,t)$, $w^X(r,z,t)$ is superposed on the base flow $(p, W(r,t))$, according to the *small perturbation method*. Attention is restricted to axisymmetric disturbances, as they are simpler to handle theoretically. Moreover, the disturbances generated in the experiments seem to be axisymmetric. Let

$$u^X = u(r,t)\exp(i\alpha z), \quad v^X = v(r,t)\exp(i\alpha z), \quad w^X = w(r,t)\exp(i\alpha z).$$

(α is the wavenumber.) The classical linearized Navier–Stokes equations read as follows, if viscosity is neglected:

$$\frac{\partial}{\partial t'}[DD^X - k^2]u' + ik\frac{h_0}{R}\left\{W'[DD^X - k^2]u' - u'\left(\frac{\partial^2 W'}{\partial r'^2} - \frac{1}{r'}\frac{\partial W'}{\partial r'}\right)\right\} = 0, \quad (19)$$

$$\frac{\partial}{\partial t'}v' + ik\frac{h_0}{R}v'W' = 0, \quad w' = \frac{i}{k}D^X u', \quad (20), (21)$$

where
$$u' = \frac{u}{\omega_p h_0}, \quad v' = \frac{v}{\omega_p h_0}, \quad w' = \frac{w}{\omega_p h_0}, \quad k = \alpha R,$$

$$D = \frac{\partial}{\partial r'}, \quad D^X = \frac{\partial}{\partial r'} + \frac{1}{r'}.$$

The boundary condition is

$$t' > 0, \quad r' = \pm 1, \quad u' = 0.$$

The non-dimensional base flow $W'(r',t')$ is separable. We assume that such is also the case for the perturbation velocity components.

First taking into account the component u', let

$$u'(r',t') = \sum_{n=1}^{\infty} g_n(r')j_n(t').$$

Should this relation be introduced into (19), one would obtain equations of the form

$$\left(\frac{d^2 g_n}{dr'^2} + \frac{1}{r'}\frac{dg_n}{dr'} - k^2 g_n\right)\left(ik\frac{h_0}{R}W'j_n + \frac{dj_n}{dt}\right) - ik\frac{h_0}{R}g_n j_n F(W') = 0,$$

where
$$F(W') = \frac{\partial^2 W'}{\partial r'^2} - \frac{1}{r'}\frac{\partial W'}{\partial r'}.$$

Let
$$Lg_n = \left(\frac{d^2 g_n}{dr'^2} + \frac{1}{r'}\frac{dg_n}{dr'} - k^2 g_n\right) - \frac{ikg_n j_n F(W')h_0/R}{dj_n/dt + ikj_n W'h_0/R} = 0.$$

The integral $\int_0^1 [(Lg_n)\bar{g}_n - (\bar{L}\bar{g}_n)g_n]\,r'\,dr' = 0$ (an overbar denotes a conjugate complex quantity) can be written, assuming j_n real, as

$$2ik\frac{h_0}{R}j_n\frac{dj_n}{dt}\int_0^1 \frac{g_n\bar{g}_n F(W')}{(dj_n/dt)^2+(h_0kW'j_n/R)^2}r'\,dr' = 0.$$

Thus, either $j_n = 0$, or $dj_n/dt = 0$, or (*condition* (i)) $F(W') = 0$ somewhere in the interval $0 \leqslant r' \leqslant 1$. It is easy to see that this result remains unchanged with j_n complex. Condition (i) is thus necessary for the existence of amplified disturbances u'. It can be shown that a further necessary condition is that W'. $F(W') < 0$ over an appreciable region of the interval $0 \leqslant r' \leqslant 1$. This last is termed *condition* (ii).

Now taking into account the components w' and v', (21) shows that the results obtained for u' also apply to w' and (20) shows that $v'(r', t')$ cannot be an increasing function of time. Therefore, if

$$\frac{\partial^2 W'}{\partial r'^2} - \frac{1}{r'}\frac{\partial W'}{\partial r'} \quad \text{for} \quad 0 \leqslant r' \leqslant 1$$

is reduced to zero and changes of sign (condition (i)) and

$$W'\left(\frac{\partial^2 W'}{\partial r'^2} - \frac{1}{r'}\frac{\partial W'}{\partial r'}\right)$$

is negative over an appreciable region of the interval (condition (ii)), then the free oscillatory flow can become unstable. These two conditions are simultaneously satisfied at any Ωt when $\gamma > 25$. A value of 25 of the parameter γ is therefore the limit below which the flow is always stable, and above which it can be unstable.

With regard to condition (i), it seems worth considering the particular reverse-flow profiles with points K defined by

$$W' = 0 \quad \text{and} \quad \frac{\partial^2 W'}{\partial r'^2} - \frac{1}{r'}\frac{\partial W'}{\partial r'} = 0.$$

We note the existence of a point K, whatever the value of γ, at the beginning of the reverse flow on the wall ($\Omega t = \Omega t_R, r' = 1$). For $\gamma < 25$, there is no other point K. For $\gamma = 25$, we note a point K at the end of the reverse flow on the axis of the tube. As the value of γ increases from 25, K moves from the axis to the wall, and occurs earlier and earlier. Thus, for $\gamma = 260$, the point K corresponds to $\Omega t = 0{\cdot}9\pi$ and to $r' = 0{\cdot}9$.

4. Experimental investigation

Experiments are conducted in two vertical U-shaped tubes 1 cm and 2 cm in diameter and 200 cm long. Mineral oils and glycerin–water mixtures with kinematic viscosity $0{\cdot}0095 \leqslant \nu \text{ cm}^2\text{ s}^{-1} \leqslant 1{\cdot}255$ are used as test fluids. The similarity parameter range investigated is

$$2{\cdot}04 \leqslant \gamma \leqslant 260 \quad \text{and} \quad 2 \leqslant h_0/R \leqslant 50.$$

4.1. *Velocity measurement*

All measurements are made with hot-film straight velocity probes operated with a DISA constant-temperature anemometer 55 D 01 at 5 % overheat. The probe response and the piezo-quartz sensor response (making it possible to calculate the angular frequency) are recorded simultaneously on an oscillograph, and with a polaroid camera. Steady probe calibrations are performed with two experimental arrangements. In the first instance, along the axis of a channel filled with the used fluid, a carriage on which the probe has been fitted is moved in a parallel direction at a constant speed. In the second, steady velocities are generated by rotating liquid in an open vessel on a turn-table. In both cases, the response of the probes whose sensing element is lowered into the liquid makes it possible to draw the calibration curves. The behaviour of the probe in an unsteady flow is studied (Seed & Wood 1970) with an oscillator, which produces a periodic motion along an arc concentric with the rotating fluid. In the conditions of the experimental investigation, the errors introduced when using the steady calibration curves are less than 5 %.

In each of the experiments carried out, corresponding to a chosen value of γ and a chosen value of h_0/R, the point velocity distribution as time progresses is successively recorded at 21 points on the diameter of a given cross-section of the U-tube. The instantaneous velocity profiles are derived from these records, at several values of $\omega_p t$ or Ωt. Furthermore, the response of a piezo-quartz sensor, which permits calculation of the period, is registered on each photograph.

4.2. *Presentation and discussion of results*

The analysis of the signal resulting from the piezo-quartz sensor response shows that, for a given value of γ, Ω is constant during the successive oscillations of the fluid column, and independent of h_0/R. Visual examination and the analysis of the point velocity distribution records, and of the instantaneous velocity profiles, enable us to state the following results.

(i) Depending on γ, h_0/R and r/R, the velocity wave forms are undisturbed (see e.g. figure 12, plate 1) or disturbed over a more or less extended portion of the successive oscillations (see e.g. figure 13(*c*), plate 2, or figure 15(*c*), plate 4). Observed disturbances should be divided into two types. Those of relatively low frequency (termed DL), which have the appearance of a Tollmien–Schlichting instability, are present on the records as oscillations around the velocity wave form (see e.g. figure 15, plate 4). They represent a transitional condition. Those of high frequency (termed DH) are superposed on the DL disturbances. They are representative of turbulent flow (figure 13(*c*), plate 2). For a chosen experiment, the flow can be successively laminar, transitional, turbulent and again laminar. The duration of each regime is a function of γ, h_0/R and r/R.

(ii) For a chosen value of γ, the instantaneous velocity amplitude is, at a chosen r/R and Ωt, an increasing function of h_0/R.

(iii) When the flow is laminar, the form of the instantaneous velocity profiles depends on γ only.

(iv) In a chosen experiment, the instantaneous velocity profiles are identical

in all cross-sections whose distance from the end of the fluid column is more than 2 cm. We have used this result in the theoretical analysis.

(v) There are several types of flow, depending on the value of γ. First, the flow is aperiodic when $\gamma \leqslant 4$. Second, it is oscillatory when $\gamma > 4$. Also, three possible oscillatory regimes can be distinguished.

(*a*) There is a regime, $4 < \gamma \leqslant 28$, in which the signal is undisturbed whatever the value of h_0/R. The flow is then laminar (figure 12, plate 1). For a value of γ the instantaneous experimental velocity profile is unique, whatever the value of h_0/R, and as seen in figure 5, the agreement between the unique experimental profile and the corresponding theoretical profile is excellent.

(*b*) There is a regime, $\gamma > 46$, in which, based on the value of h_0/R, DH disturbances are present during at least the whole first down motion of the fluid column, showing therefore the characteristics of a turbulent flow (figure 13(*c*), plate 2). As a matter of fact, there is, for each value of γ, a value of h_0/R, $(h_0/R)_{c_1}$, below which the flow is laminar. For values of h_0/R slightly higher than $(h_0/R)_{c_1}$, a DL disturbance is visible close to $\Omega t = \frac{3}{2}\pi$. When h_0/R increases DL, then DH disturbances, whose amplitude and frequency go on increasing, can be seen in the flow earlier and earlier before $\frac{3}{2}\pi$, and later and later after $\frac{3}{2}\pi$ (figures 13(*a*), (*b*), plate 2). For $(h_0/R)_{c_2}$, the flow is highly disturbed, and shows the characteristics of a turbulent flow during the whole first down motion. When h_0/R increases beyond $(h_0/R)_{c_2}$, the flow always remains laminar until the beginning of the reverse flow, but the number of oscillations during which the flow is completely turbulent increases. When the up motion of an oscillation is completely turbulent, so is the down motion; and there is an up–down coupling. These couplings start with the second oscillation; and, for a given γ, as h_0/R increases, they affect more and more oscillations (figure 13(*c*), plate 2). $(h_0/R)_{c_1}$ and $(h_0/R)_{c_2}$ depend on γ. On the axis of the tube, this dependence appears to be well represented by

$$(h_0/R)_{c_1} = 175\gamma^{-0{\cdot}6}, \quad (h_0/R)_{c_2} = 450\gamma^{-0{\cdot}6}. \tag{22}$$

For a given value of γ, if $h_0/R < (h_0/R)_{c_1}$, the instantaneous velocity profile is unique whatever the value of h_0/R. But, if $h_0/R \geqslant (h_0/R)_{c_1}$ to each value of h_0/R there corresponds an instantaneous velocity profile. The experimental profiles and the corresponding theoretical profile are qualitatively similar during the first up motion. On the other hand, from the beginning of the first down motion, the experimental and corresponding theoretical profiles are qualitatively similar only if the flow is not turbulent. Figure 6 ($\gamma = 177$) shows typical experimental turbulent profiles, with a central flat part. Such is the case with $h_0/R = 25$ and $\Omega t = \frac{3}{2}\pi$.

(*c*) There is an intermediate regime $28 < \gamma \leqslant 46$, in which, when h_0/R increases from $(h_0/R)_{c_1}$, disturbances are observed earlier and earlier in the flow, before $\Omega t = \frac{3}{2}\pi$, up to $\Omega t = \Omega t_2$. But there is never any disturbance in the decelerated phase of the first down motion (figure 15, plate 4).

The successive up motions are laminar up to Ωt_R, corresponding to the beginning of the reverse flow; and at Ωt_R the velocity wave forms are disturbed, whatever the value of r/R, if h_0/R is large enough. Furthermore, there is never

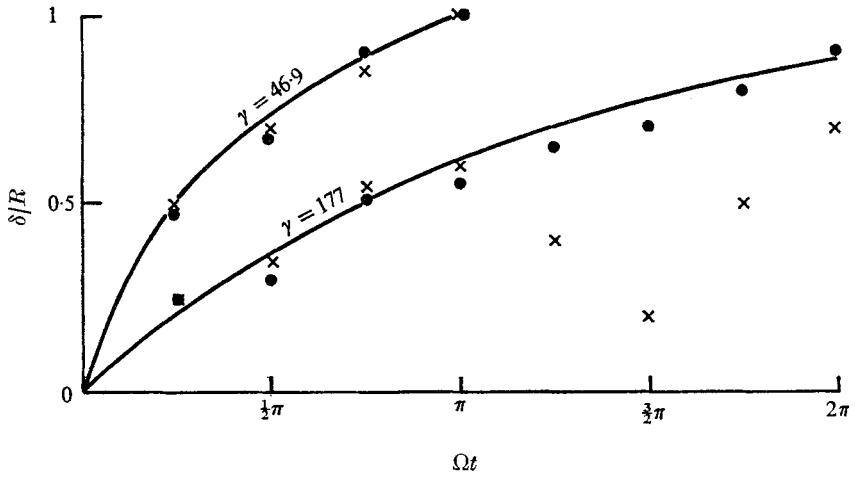

FIGURE 16. Boundary-layer relative thickness δ/R as a function of Ωt. ——, theory (γ = 46·9 or 177). Experiment, h_0/R: ●, 4; ×, 25.

any DH disturbance in velocity wave forms. As shown in figure 7, the experimental profile corresponding to $\gamma = 42$, $h_0/R = 4$ is in good agreement with the theoretical. Finally, in aperiodic flow, the flow is laminar, and the results concerning the velocity profiles are the same as in the first regime (figure 4).

As regards the boundary layer, we note in figure 16 that the curves representing the evolution as time progresses of the experimental boundary-layer relative thickness δ/R are quite in agreement with the corresponding theoretical curves given by (15), when the flow is laminar. When the flow is turbulent, the experimental points deviate further from the corresponding theoretical curve. This is the case at $\gamma = 177$ and $h_0/R = 25$ when $\Omega t \simeq \frac{3}{2}\pi$. The experimental results are therefore quite in agreement with the corresponding computer solutions when the flow considered is laminar. The disturbances observed in the experiments may now be examined in somewhat more detail.

4.3. *Disturbance studies*

Let us first consider DL disturbances. The results of the visual examination of the velocity records are highly suggestive of the fact that the DL disturbances are generated in the boundary layer during the reverse flow, then transmitted to the inviscid core. Also they suggest that this happens for a given value of γ (or h_0/R) much more quickly than h_0/R (or γ) increases. On the other hand, the amplitudes of these disturbances decrease at the end of the boundary layer.

In fact, whatever the value of γ and h_0/R, there is never any disturbance during the first up motion before Ωt_2, corresponding to the beginning of the reverse flow. Moreover, in the first regime, for which reverse flow occurs when velocity profiles are fully developed ($\Omega t_2 > \Omega t_l$), the flow is not disturbed. In the intermediate regime, considering e.g. $\gamma = 42$, $h_0/R = 50$ (figure 15, plate 4), at $\Omega t_2 \simeq \frac{3}{4}\pi$ where $\delta/R \simeq 1$, the flow is disturbed in the whole section, and DL disturbances of decreasing amplitudes are visible up to $\frac{3}{4}\pi$ close to the wall,

and $\frac{3}{2}\pi$ on the axis. In the second regime, considering e.g. $\gamma = 260$, $h_0/R = 25$ (figure 14, plate 3), at $\Omega t_2 \simeq \frac{3}{4}\pi$ where $\delta/R \simeq 0{\cdot}35$, the flow is disturbed only close to the wall, the whole section is disturbed at $\Omega t \simeq \frac{5}{4}\pi$, and disturbances are visible up to $\Omega t = 5\pi$ ($\Omega t_l = 3\pi$).

The points K,

$$W' = 0, \quad \frac{\partial^2 W'}{\partial r'^2} - \frac{1}{r'}\frac{\partial W'}{\partial r'} = 0,$$

given by the stability criterion established in §3.5, could be considered as the origin of DL disturbances. So DL disturbances should be generated in the second regime at Ωt_R on the wall and at Ωt ($\Omega t_2 < \Omega t < \pi$ for the first oscillation) in the boundary layer, and in the intermediate regime at Ωt_R on the wall only. (In the latter case, the second point K is not in the boundary layer.)

Finally, in an experimental study of the velocity distribution and transition to turbulence in the aorta, Nerem, Seed & Wood (1972) suggest that the boundary layer plays a dominant role in the generation of the disturbances observed in their experiments. Furthermore, disturbances appear immediately after peak systole (i.e. at the beginning of the reverse flow). As regards the DH disturbances, their generation seems to occur in the central core. In fact, for each value of γ, there is a value of h_0/R below which no DH disturbance ever occurs. For a value of h_0/R slightly higher, DH disturbances appear on the axis of the tube and near $\Omega t = \frac{3}{2}\pi$, corresponding to the peak velocity. Then the lifetime of these disturbances, and the radius of the core they affect are increasing functions of h_0/R. Although there is no proof, another possible explanation of DH disturbances during the down motions is the instability of the free surface. As regards the characteristic parameters of the laminar–turbulent transition, taking

$$\mathscr{R} = W_{\max} R/\nu$$

($W_{\max}$ is the maximum velocity as time progresses), we can define, using (22), a critical Reynolds number

$$\mathscr{R}_{c_1} = 175\gamma^{0{\cdot}4} W_{\max}/(\omega_p h_0). \tag{23}$$

This is a function of just the parameter γ. Consequently, the Reynolds number, alone, cannot determine the structure of the flow. Two parameters chosen from the group $\mathscr{R}$, γ, h_0/R are necessary to do so. It seems interesting to compare the critical Reynolds number (23) with those given in Nerem *et al.*:

$$\begin{aligned} \mathscr{R}_{c_1} &= 150(R^2\Omega/\nu)^{0{\cdot}5} \quad \text{(ascending aorta)}, \\ \mathscr{R}_{c_1} &= 250(R^2\Omega/\nu)^{0{\cdot}5} \quad \text{(descending aorta)}. \end{aligned} \tag{24}$$

For the values of the frequencies of oscillations considered by these authors, our analysis gives $W_{\max}/(\omega_p h_0) \simeq 1{\cdot}05$, $\omega_p/\Omega \simeq 1$. We obtain, for (23),

$$\mathscr{R}_{c_1} = 190(R^2\Omega/\nu)^{0{\cdot}4}.$$

This result is in good agreement with (24).

4.4. *Visualizations of the flow*

Flow visualizations were made, using a working fluid with particular optical properties: e.g. a solution of carbon bisulphide, acetone and peanut oil, which made it possible to see disturbances inside the fluid column. With this solution, by the quantity determination of the constituents, it was possible to obtain various kinematic viscosities, then various values of γ. Films and photographs were taken in several parts of the fluid column, during the motion. Analysis of these records shows that, for a working section distant from the free surface, vortices are present only if

$$\gamma > 25 \quad \text{and} \quad h_0/R > (h_0/R)_{c_3},$$

$(h_0/R)_{c_3}$ being a decreasing function of γ, such that

$$(h_0/R)_{c_3} < (h_0/R)_{c_1}.$$

For
$$(h_0/R)_{c_3} < (h_0/R) < (h_0/R)_{c_1},$$

vortices are produced in the fluid column during the first down motion, and are damped as time progresses. For

$$(h_0/R)_{c_1} < h_0/R < (h_0/R)_{c_2},$$

these vortices generate a more or less disturbed flow, during the first down motion when the velocity is the highest. For

$$h_0/R > (h_0/R)_{c_2}$$

the flow is turbulent during the whole first down motion, but always laminar during the greater part of the first up motion (figure 17, plate 5). Thus, the results of examination of the velocity waves are confirmed by these visualizations.

Now, if we consider the flow in the vicinity of the free surface, whatever the value of γ, for any value of h_0/R higher than $(h_0/R)_l$, $\gamma(h_0/R)_l = 260$, i.e.

$$\mathscr{R} = W_{\max} R/\nu \simeq 260,$$

a ring vortex (figure 18, plate 6) is formed in the early stage of the first down motion, develops to fill the whole cross-section of the tube, then destroys itself.

It is worth noting that Hughes & Gerrard (1971) showed (in an experimental study of the flow relative to a piston and a free surface started from rest) that a ring vortex is produced just below the surface when the Reynolds number is higher than 225. In a theoretical study, Gerrard (1971) had shown that the ring vortex is present in computed flow only if the flow is at each time disturbed randomly. As far as our study is concerned, on account of the impulsive change of the motion, the free surface is disturbed for $\Omega t \simeq \pi$. Furthermore, the equivalence, between the process of an impulsive change of the sense and an impulsive start of the motion, leads us to think that the existence of the ring vortex is the result (Telionis & Tsahalis 1974) of the superposition of the inviscid flow generated by the impulsive change on the existing viscous fluid, and that our study is similar to Gerrard's.

Finally, the free surface is unstable when acceleration is directed towards the liquid (Taylor 1950; Benjamin & Ursell 1954). Hence, for the present study, in a down motion the free surface is unstable.

5. Conclusion

Analysis of theoretical and experimental results on oscillatory free motion shows that this flow is not governed by just one similarity parameter, as is the case in steady flows, but by two, chosen from the group γ, h_0/R, $\gamma h_0/R$ (where $\gamma h_0/R$ is a Reynolds number). We shall add that we have the feeling that this result can be extended to some other unsteady flows. More precisely, and though the free oscillatory flow studied here differs markedly from blood flow in arteries, we think we are justified in stating that our results will provide further insight into arterial blood flow.

REFERENCES

BATCHELOR, G. K. 1967 *An Introduction to Fluid Dynamics*. Cambridge University Press.
BATCHELOR, G. K. & GILL, A. E. 1962 *J. Fluid Mech.* **13**, 529.
BENJAMIN, T. B. & URSELL, F. 1954 *Proc. Roy. Soc.* A **225**, 505.
CLARION, C. 1955 *Publ. Sci. Tech. du Ministère de l'Air*, no. 303.
CONRAD, P. W. & CRIMINALE, W. O. 1965*a* *Z. angew. Math. Phys.* **16**, 233.
CONRAD, P. W. & CRIMINALE, W. O. 1965*b* *Z. angew. Math. Phys.* **16**, 569.
GERRARD, J. H. 1971 *J. Fluid Mech.* **50**, 625.
HOILAND, E. 1953 *Geophys. Publ. Norske Videnskaps. Akad. Oslo*, **18** (9), 1.
HUGHES, M. D. & GERRARD, J. H. 1971 *J. Fluid Mech.* **50**, 645.
NEREM, R. M., SEED, W. H. & WOOD, N. B. 1972 *J. Fluid Mech.* **52**, 137.
RAYLEIGH, LORD 1895 *Scientific Papers*, vol. 3, p. 594. Cambridge University Press.
SEED, W. A. & WOOD, N. B. 1970 *Cardiovascular Res.* **4**, 253.
SEXL, T. 1930 *Z. Phys.* **61**, 349.
TAYLOR, G. I. 1950 *Proc. Roy. Soc.* A **201**, 192.
TELIONIS, D. P. & TSAHALIS, D. T. 1974 *A.I.A.A. J.* **12**, 614.
UCHIDA, S. 1956 *Z. angew. Math. Phys.* **7**, 404.
VALENSI, J. 1947*a* *CRAS* **224**, 446.
VALENSI, J. 1947*b* *CRAS*, **224**, 532.
VALENSI, J. 1947*c* *CRAS*, **224**, 893.
WOMERSLEY, J. R. 1955 *Phil. Mag.* **46** (7), 199.

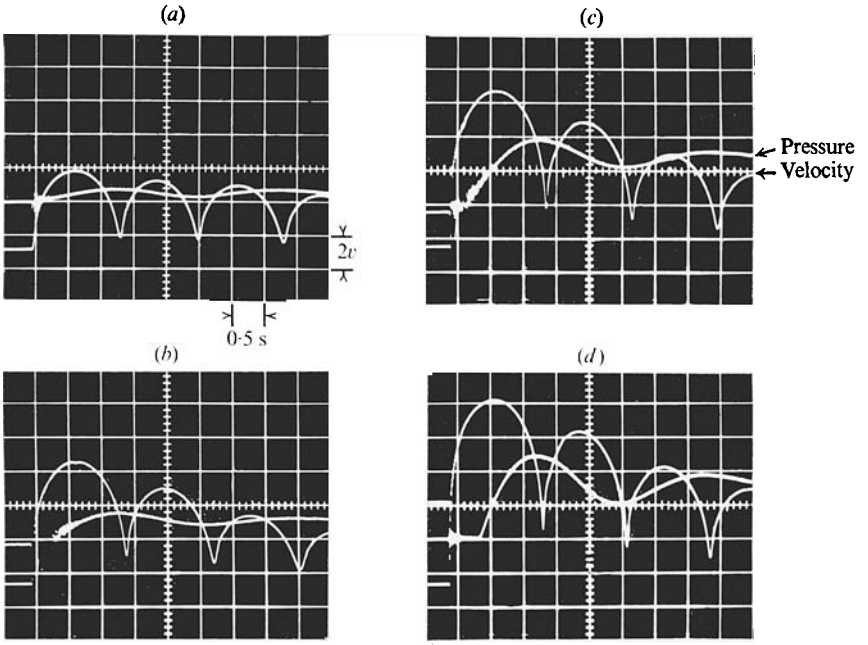

FIGURE 12. Point velocity records, $\gamma = 15{\cdot}3$ (first regime), $r/R = 0$. h_0/R: (*a*) 4; (*b*) 10; (*c*) 25; (*d*) 50.

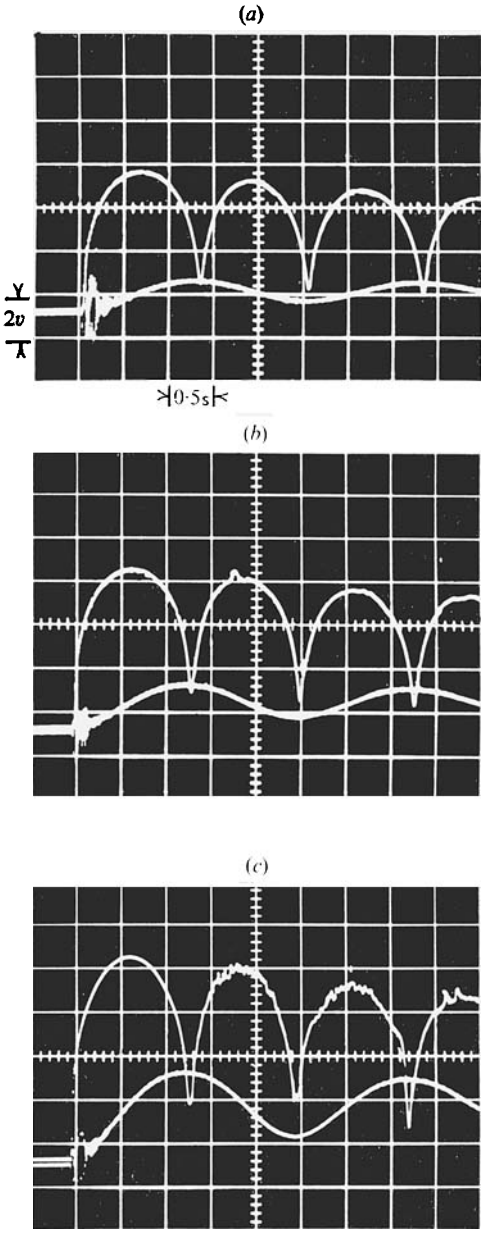

FIGURE 13. Point velocity records, $\gamma = 177$ (second regime), $r/R = 0$. h_0/R: (*a*) 8; (*b*) 15; (*c*) 25.

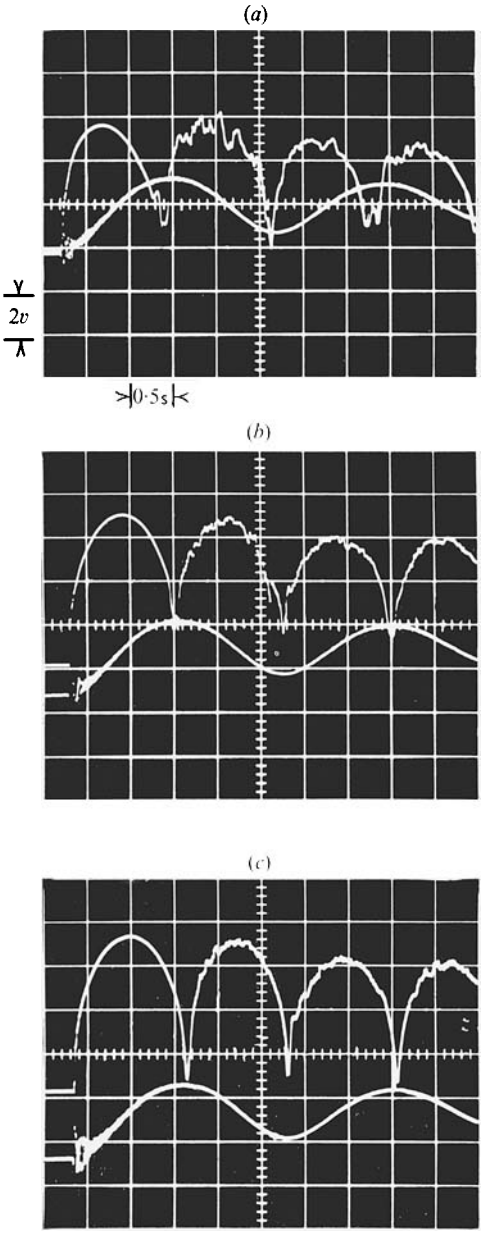

FIGURE 14. Point velocity records, $\gamma = 260$ (second regime), $h_0/R = 25$. r/R: (*a*) 0·9; (*b*) 0·6; (*c*) 0·2.

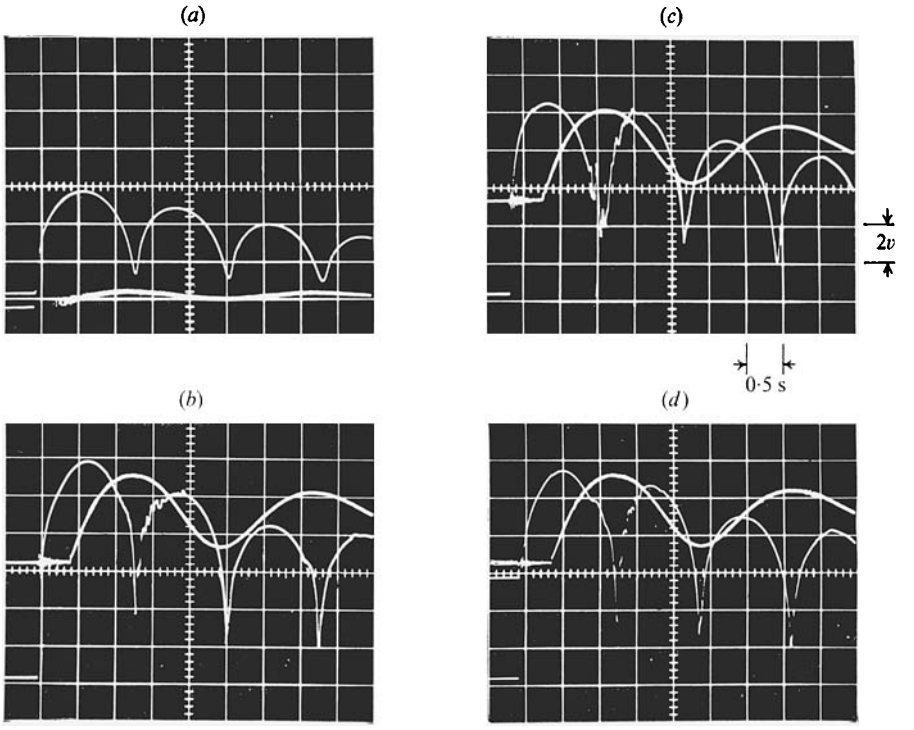

FIGURE 15. Point velocity records, $\gamma = 42$ (intermediate regime).

	(a)	(b)	(c)	(d)
r/R	0	0	0·9	0·6
h_0/R	20	50	50	50

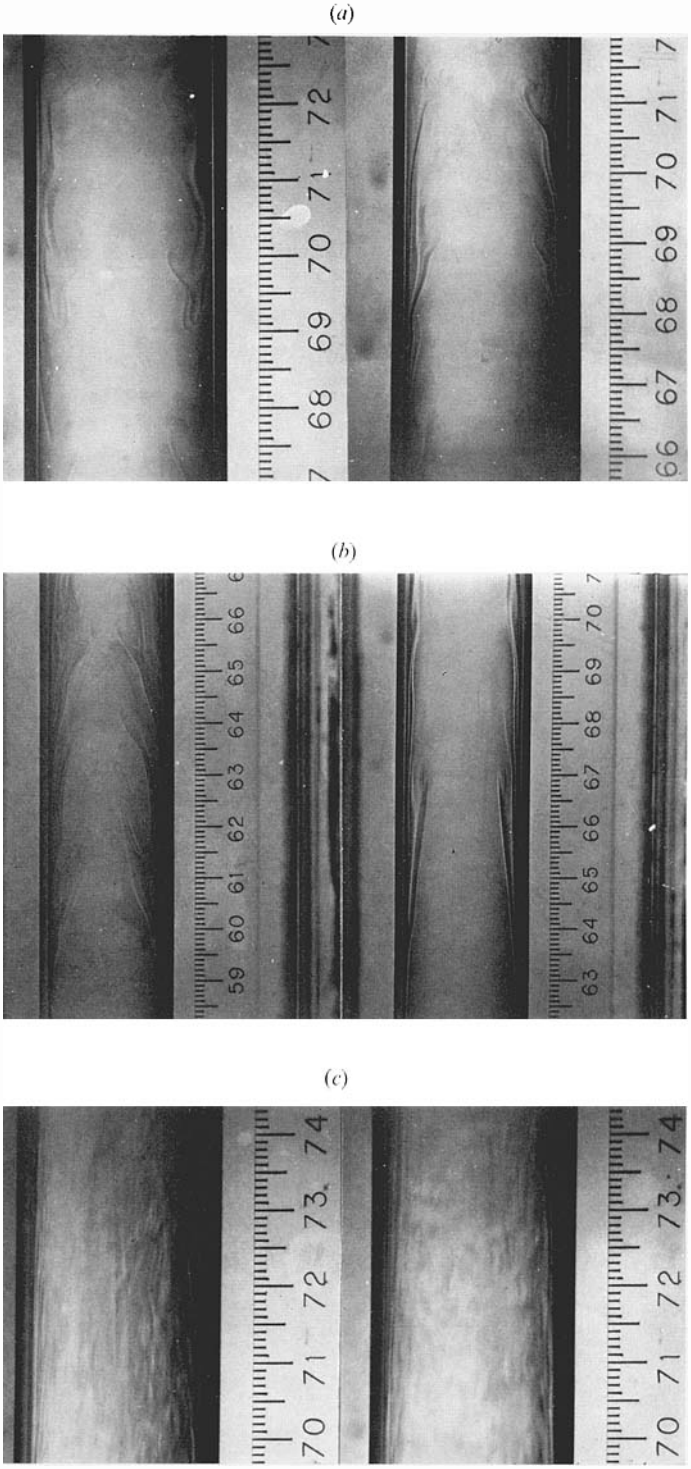

FIGURE 17. Visualization in the fluid column, $\gamma = 66$. h_0/R: (*a*) 9 (up motion (ii)); (*b*) 20 (up motion (ii)); (*c*) 50 (down motion (i)).

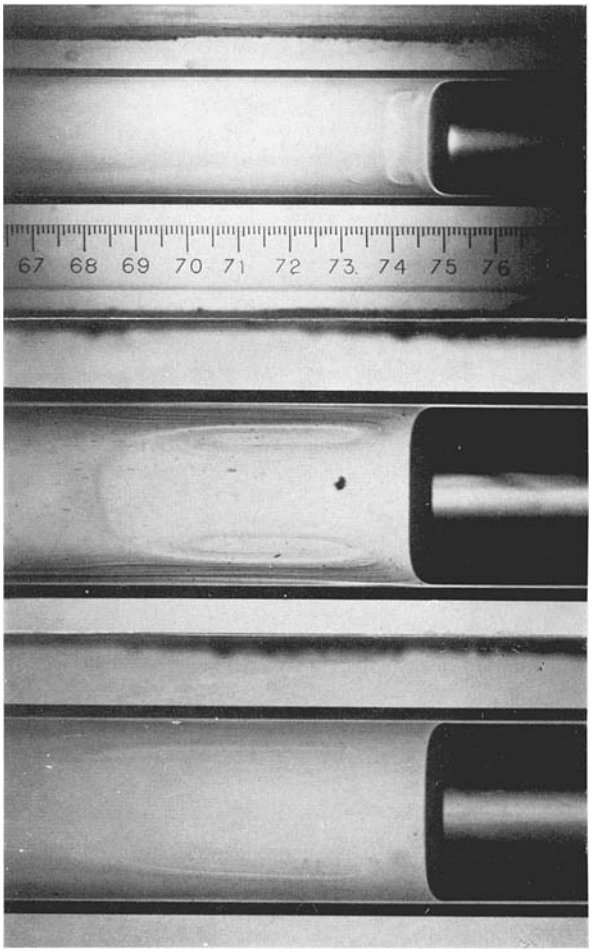

FIGURE 18. Visualization of the evolution of the ring vortex below the free surface, $\gamma = 25$, $h_0/R = 20$, down motion (i).